## CONFERENCE PRE-PRINT

# SIMULATIONS OF THE INTERACTIONS BETWEEN ELMS AND EDGE TURBULENCES ON FUSION REACTOR SCALE FACILITY

T.Y. Xia

Institute of Plasma Physics, Chinese Academy of Sciences

Hefei, China

Email: xiaty@ipp.ac.cn

H.M. Oi

Institute of Plasma Physics, Chinese Academy of Sciences, University of Science and Technology of China Hefei, China

X.X. He

Institute of Plasma Physics, Chinese Academy of Sciences

Hefei, China

Y.L. Li

Institute of Plasma Physics, Chinese Academy of Sciences

Hefei, China

B. Gui

Institute of Plasma Physics, Chinese Academy of Sciences

Hefei, China

Y.D. Yu

Institute of Plasma Physics, Chinese Academy of Sciences, University of Science and Technology of China Hefei, China

H. Yu

Institute of Plasma Physics, Chinese Academy of Sciences, University of Science and Technology of China Hefei, China

Y.H. Zhu

Southwest Jiaotong University, Chengdu, China

Chengdu, China

**EAST Team** 

Institute of Plasma Physics, Chinese Academy of Sciences

Hefei, China

# **Abstract**

The edge localized modes (ELMs) are considered as an important potential damage to divertors and first walls on the future fusion facilities. This paper exhibits the ELM simulations based on the ITER and CFETR like fusion reactor. The pedestal is obtained with EPED1 model. Based on the scaling of pedestal collisionality, the ELM should be Type-I. The simulations with resistive peeling-ballooning mode (PBM) model prove this result. However, when the full 2-fluid model, which includes the ion temperature gradient (ITG) and drift Alfven wave (DAW) modes, is applied for the simulations, the ELM will be suppressed dramatically, around 80% decreased on ELM size. The detailed analysis shows that this suppression is not caused by the finite Lamore radius effects in the linear phase. The nonlinear interactions between electro-magnetic edge electron turbulence and ELMs are the key effects. In the fusion reactor like pedestal, the high beta leads to a high level of electromagnetic turbulence, and the low rotation leads to the small damping. Therefore, this work indicates that the pedestal in reactor-like tokamak predicted by Type-I ELM model may not results in large ELM. This will give help for the solutions of the large transient heat flux issues for ITER.

## 1. INTRODUCTION

The high-confinement mode (H-mode) is considered to be the main operation scenario for ITER and future fusion reactors. However, the larger edge transport barrier in H-mode will cause the periodic crashes of temperature and density profiles, which is named as edge localized mode (ELM). The Type-I ELM, which is triggered by the coupling of peeling and ballooning modes [1], is the most serious risk to the safety of the first wall and divertors of tokamaks [2]. Therefore, the active control of ELMs is of great significance for the developing of high performance operations for the present and future tokamaks. Various methods have been investigated for the active control of ELMs in tokamaks. Resonant magnetic perturbations (RMPs) have been widely applied to suppress and mitigate ELMs, in DIII-D, KSTAR, JET and EAST [3-6]. The edge topological changes, resulting from the nonlinear plasma response, play a key role in the suppression of ELMs with RMPs. Other methods, such as pellet injection, supersonic molecular beam injection (SMBI), are able to enhance transport at the plasma boundary region through the small disturbances [7]. The completely ELM-free regime has also been obtained in NSTX and EAST by the injection of lithium (Li) into edge plasmas [8, 9].

Besides these, other ELM mitigation and suppression methods are also proved effective. For example, in recent EAST experiments, the lower-hybrid waves (LHWs) provide a way to suppress or mitigate ELMs through the helical current filaments (HCFs), which is driven by LHWs in the SOL region. The HCFs can generate an important change in the magnetic topology in the plasma edge region, similar to the effects of RMPs[5, 10]. The simulations of ELM nonlinear evolutions with the modelled HCF with BOUT++ show that HCF can decrease the growth rate and enhance the mode coupling. The energy inverse cascade is constrained by HCF, which leads to the absence of dominant filamentary structures and the mitigation of ELM. Ion-cyclotron resonant heating (ICRH) is found to be another effective way to suppress ELMs in EAST [11]. The external E × B velocity shear near the pedestal top and the scrape-off-layer (SOL) induced by the RF sheath potential of ICRH plays the key role in ELM suppression. A positive correlation between the RF sheath and the E × B shear rate in SOL are observed in experiments, and it is also proved by simulations [12]. These findings suggest a new simple approach to access the ELM suppressed regimes in plasma with low torque input as CFEDR discharges.

The initial-value BOUT++ framework has successfully simulated the nonlinear evolutions of ELMs [13, 14]. The elm-6f module has been developed to simulate ELM crashing in both shifted-circular and X-point geometries [15,16]. The divertor heat fluxes during an ELMy H-mode in DIII-D has been studied by this model [17]. The collapse of the density profile in the width and depth of electron density ne during the burst of ELMs is reproduced by this module. The growth process of the profiles for the heat flux at divertor targets during ELMs is also simulated. The asymmetric distributions of the particle flux at the upper and lower outer divertors in the EAST double-null geometry is also reproduced by this model [16]. This module is also used for the studies of edge turbulence, such as the quasi-coherent mode (QCM) in DIII-D and the weak coherent mode (WCM) in C-Mod [18, 19]. The theoretical and simulation results of a gyro-Landau-fluid (GLF) extension of the BOUT++ code are summarized in [20, 21, 22], which contributes to increasing the physical understanding of ELMs. Therefore, this module is used in this paper for the understanding of the ELM behaviours in future tokamaks..

In the previous simulations on ELM mitigation and suppression, we have found that the existence of turbulence is able to mitigate or even suppress ELMs in EAST [14, 23]. Using an imposed perturbation added as a coherent mode (CM) into the ELM simulation, CM enhances the three-wave nonlinear interactions in the pedestal and reduces the phase coherence time (PCT) between the pressure and potential [23]. In this way, the fluctuations tend to be 'multiple-mode' coupling. The competitions of free energy between these multiple modes lead to the lack of obvious filament structures and the decreased the energy loss. Not only the electro-static turbulence has this mitigation effect, the electro-magnetic fluctuations, which is contributed by the filamentary current in SOL generated by Lower Hybrid waves (LHWs) on EAST, also present the similar influence. The above reveals that there is a competitive relationship between turbulence and ELMs, and edge turbulence does effectively reduce ELM energy loss.

This paper exhibits the ELM mitigations by self-consistently generate turbulence for the fusion reactor size facilities. Besides ITER, a JET-like compact tokamak and a CFETR-like reactor are studied for the simulations on ELM behaviours, in which the pedestal structures are predicted by EPED1.6 model. Although these pedestals are unstable to ideal Peeling-Ballooning modes (IPBM), the simulations with 6-field 2-fluid model in BOUT++ framework [15, 17], which includes non-ideal effects such as ion diamagnetic effects, Drift Alfven wave (DAW), ion acoustic waves, resistivities, thermal conductions, etc., exhibit small ELM regimes. The high pedestal profiles in the reactor scale facilities leads to strong turbulent transport, which interrupts the normal growth and change the nonlinear mode spectrum of ELM. The Type-I ELM could not get grown and turn to a small one, or even turbulent behaviours.

#### 2. ELM SIMULATIONS FOR ITER PFPO SCENARIOS

The simulation equilibria of the ITER 5MA PFPO-1 scenario and 7.5MA PFPO-2 scenario with lower plasma current, magnetic field and density consist of g-files and p-files generated using CORSICA[24]. Hydrogen (H) is the main ion species for the PFPO-1 scenario and helium (He) for the PFPO-2 scenario. The simulation domain is set as  $\psi_N$ =0.9~1.05, where  $\psi_N$  is normalized poloidal magnetic flux. The resolution of both equilibria is 260×64 in the x, y direction. The temperature  $T_{e0}$  is similar to  $T_{i0}$  for PFPO-2 and the temperature  $T_{e0}$  is almost two times larger than  $T_{i0}$  for PFPO-1. The  $n_{e0}$ = $n_{i0}$  is applied for PFPO-1 while the  $n_{e0}$ = $2n_{i0}$  is applied for PFPO-2 due to the different main ion species and no impurities considered. The positions of the peak value of current and pressure gradient are at  $\psi_N$ =0.98.

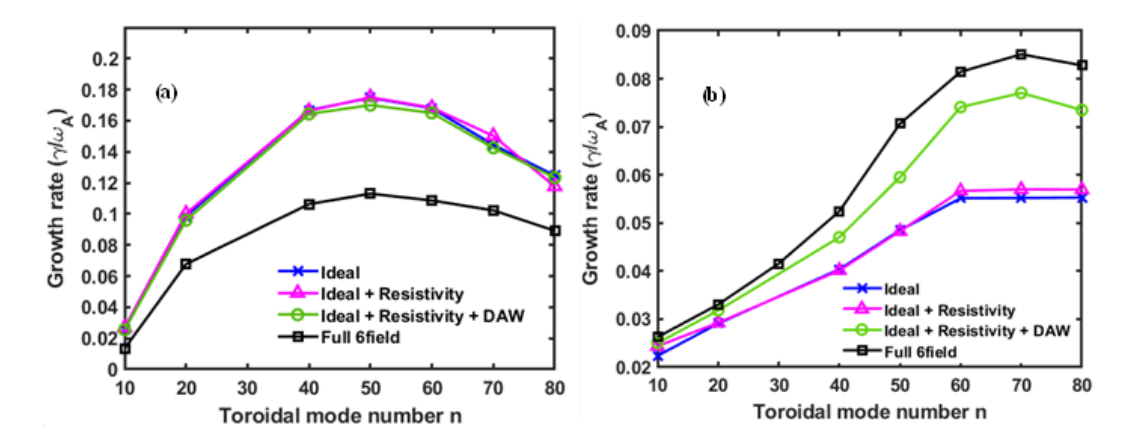


Figure 1 Linear growth rate with different reduced modules of: (a) ITER 5MA PFPO-1 scenario; (b) ITER 7.5MA PFPO-2 scenario

The linear analysis, as illustrated in figure 1, consistently reveals the trigger mechanism and characteristics of the equilibrium. When the Spitzer resistivity is considered, the linear growth rates are almost covered that of the ideal PB mode. The comparison of these curves reveals that the equilibrium of PFPO-1 in figure 3(a) is primarily destabilized by the ideal ballooning, while the equilibrium of PFPO-2 in figure 3(b) is destabilized by both ideal PB and DAW instability.

The PFPO-2 equilibrium is selected for the nonlinear turbulence simulations to investigate the influence of DAW on ELM. As shown in Figure 1, the resistivity  $\eta$  is considered as Spitzer–Härm form, and the sheath boundary conditions are applied for parallel velocity, parallel sheath current and parallel ion and electron heat fluxes on divertor targets. The energy loss ratio from the pressure channel during an ELM burst can be quantified by ELM size and is defined as  $\Delta = \Delta W_{ped}/W_{ped}$  [13]. The calculated ELM size is about 0.5% for PFPO-2, indicating a very small ELM. The simulated pressure perturbation starts to arise from the position near the peak pressure gradient, then spreads radially to both sides. Therefore, turbulence in the SOL is generated in the pedestal region and propagates through the separatrix, rather than produced by local perturbations. Since the pressure perturbation is near the boundary of plasma instability, the slight evolution of the pressure profile does not generate strong turbulence, nor does the turbulence propagate into the SOL.

Three nonlinear simulations are performed with both PB mode and DAW driving terms, and also for the cases with either one of them in the model to analyse the impact of PB and DAW instabilities on the ELM dynamics. In figure 2, plots in column 'a' are the simulation results with both PB and DAW driving. Those in column 'b' are the simulation results without DAW instability driving terms, and 'c' are without PB instability driving. Using the Fourier transform, the time evolutions of pressure perturbation at the peak gradient region at the OMP with different toroidal mode numbers during the nonlinear simulations for three cases are shown in the upper row of figure 2. The time evolutions of pressure profiles at the OMP during the ELM crash are shown in the lower row of figure 2, corresponding to the three cases. For the case 'a', the linear growth rate is large, leading to a rapid transition to the nonlinear stage. Throughout nearly the whole nonlinear phase, a visible n=0 perturbation, represented by the blue curve, is observed. This indicates that more free energy is redistributed to the zonal component, resulting in the increased energy loss. According to the results for case 'b', the linear growth rates decrease obviously after excluding the PB instability driving term. The time period before the nonlinear stage is prolonged, the zonal perturbation disappears, and the amplitude of the disturbance is reduced by nearly one order

of magnitude. There is no ELM burst and the pressure profile remains unchanged. By comparing the results of cases 'a' and 'b', we can conclude that the PB instability driving is a necessary condition for pedestal collapse. This finding is consistent with the well-established theory that PB modes trigger magnetic reconnection, which subsequently leads to the collapse of the pedestal[15,13]. The results in column 'c' of figure 2, which excludes the DAW driving term, are similar to those of case 'b'. The linear growth rates are decreased significantly and the zonal perturbation vanishes. The enhanced interactions between perturbations with different toroidal modes lead to energy dispersion and an overall reduction in disturbance amplitude, which decreases by almost one order of magnitude. Since the perturbation does not grow sufficiently to trigger an ELM before entering the nonlinear stage, there is no ELM burst and the pressure profile remains unchanged. By comparing the results in figure 2, we can find that the PB instability driving is a necessary but insufficient condition for ELM dynamics for this PFPO-2 equilibrium, and the DAW driving can strengthen the turbulence effects induced by PB modes to a certain extent.

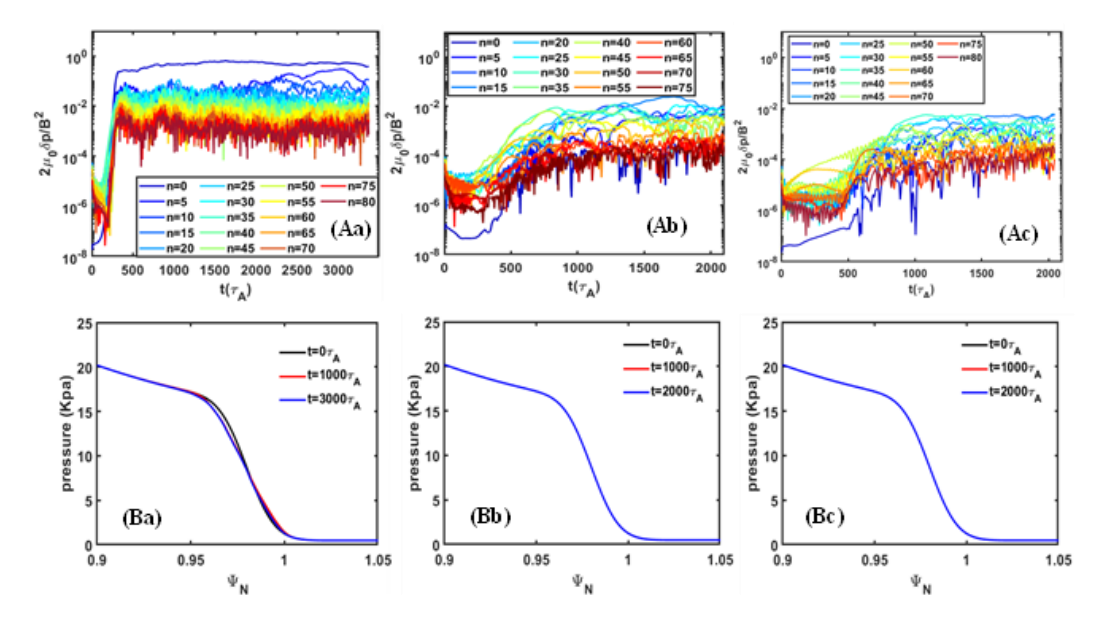


Figure 2 (A) Time evolution of pressure fluctuation for different toroidal mode numbers and (B) the radial pressure profiles at different times. The three columns are for three different linear instability drives: (Aa) and (Ba) with both PB and DAW drives; (Ab) and (Bb) with DAW drive only without PB drive; (Ac) and (Bc) with PB drive only without DAW drive.

# 3. ELM SIMULATIOSN FOR A JET-LIKE COMPACT TOKAMAK

In this section, a compact tokamak with the similar size as JET has been applied in this section for the understanding of the ELM behaviours in future facilities. The major radius is set about 3.2 m, the minor radius is around 0.9 m. The magnetic axis is R = 3.56 m, where the toroidal magnetic field is  $B_t = 6T$ . The toroidal current is  $Ip\sim7.5MA$  with the high performance scenario. The simulation domain and plasma profiles are shown in figures 3. The electron and ion temperatures at pedestal top are set to be the same as 4.3 keV, and the electron density here is around  $1.62 \times 10^{20}$  m<sup>-3</sup>.

The results of the linear analysis are shown in Figure 4. We can see that the linear instability is driven by ideal PBM, and resistivity is highly unstable which increase the growthrates obviously. The ion diamagnetic stabilizing effects are able to decrease the amplitude of the growthrates, but could not stabilize the high-n modes. The full effects of 6-field 2-fluid model do not change the growthrates of high-n modes too much, but destabilize the lown modes. If DAW is not taken into consideration, the high-n modes with n>35 are totally stabilized. From this result, we can find DAW is important to drive the high-n instabilities.

For the nonlinear simulations with the full model, the ELM size is around 0.76%, which is usually considered as a small ELM. Due to the small ELM size, or energy loss, the peak parallel heat flux towards divertor targets are 737.4MW/m². The SOL width is fitted with the Eich's scaling formula,  $\lambda_q$ =3.5mm, which is much smaller than the multi-machine scaling law. This nonlinear simulation results are interesting because the equilibrium is unstable to ideal PBM, so considering the scaling of collisionality and  $\beta_p$ , it is supposed to be a large ELM, or at least not so small one. If using ideal PBM model to simulate this equilibrium, the ELM size is 2.64%, which should be a

Type-I ELM. Therefore, we add the different non-ideal effects into the model, such as thermal conduction, gyroviscosity, parallel velocity equation and compressible terms in density and temperature equations. The conclusion is that the compressible terms play the most important stabilizing effects in this case. With compressible terms, the fluctuation amplitude is decreased by  $\sim$ 87%, and ELM size by 85%.

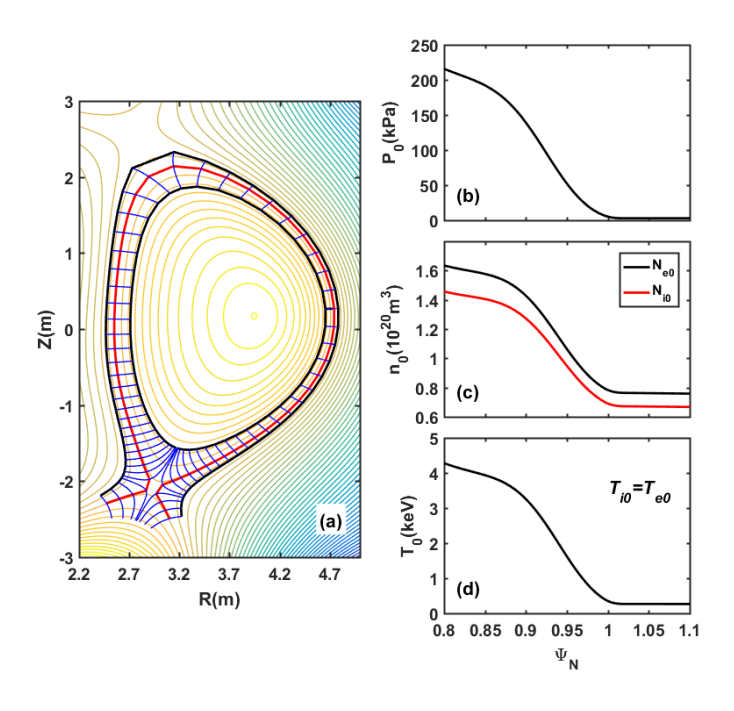


Figure 3 Panel (a):The simulation domain of the JET-size-like tokamak. (b) is the total pressure profile for the simulation. (c) electron and ion density profiles (d) electron and ion temperature profiles.

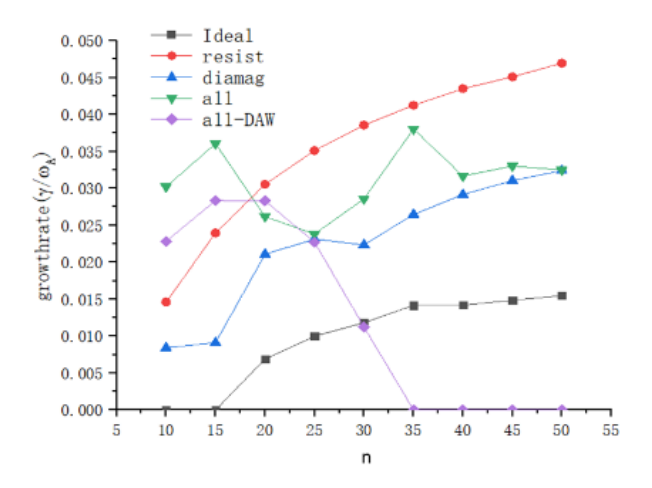


Figure 4 The linear growthrates of the equilibrium in Figure 3. The black curve represents the growthrates of ideal PBM. Red are with the Spitzer resistivity. Blue are with ion diamagnetic effects. Green curve is results with the full model, while purple one is the full model without DAW driving.

## 4. ELM SILULATIONS FOR CFEDR

For the physics design of CFEDR, we do the ELM simulations for the pedestal instabilities under 15MA operation scenario. The same model is applied for the simulations, and the input magnetic shaping are shown in Figure 5, as well as the pressure, density and temperatures. The range of the simulation domain is from  $\psi_N$ =0.9 to  $\psi_N$ =1.04. In this equilibrium, the ion and electron temperatures are set to be the same, which is different from that in Figure

4. The type of ELM can be roughly estimated as Type-I by the scaling of collisionality and  $\beta_p$ , as shown in Figure 6(b).

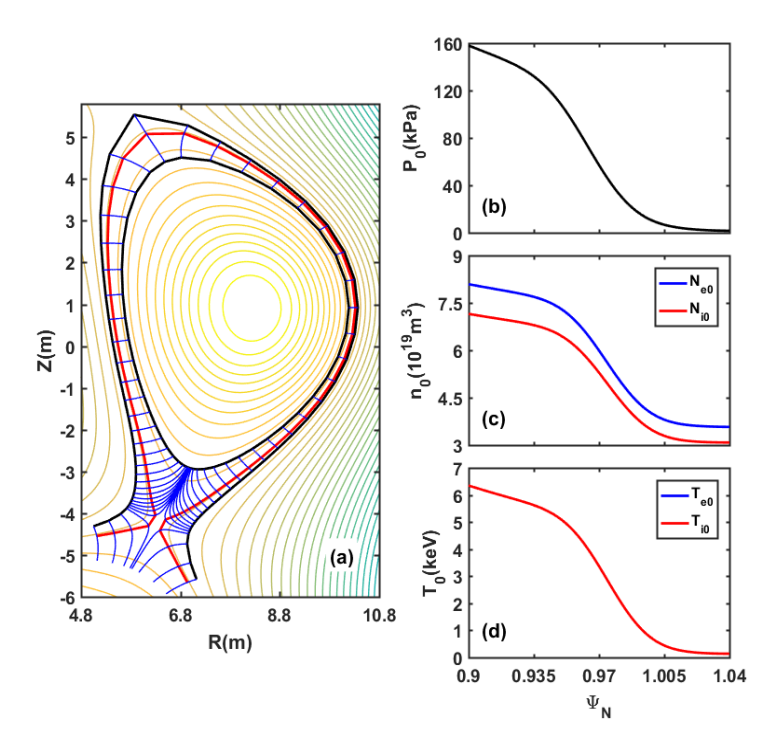


Figure 5 The simulation domain for CFEDR 15MA operation scenario. The pressure, density and temperature profiles are shown in panel (b), (c) and (d), respectively.

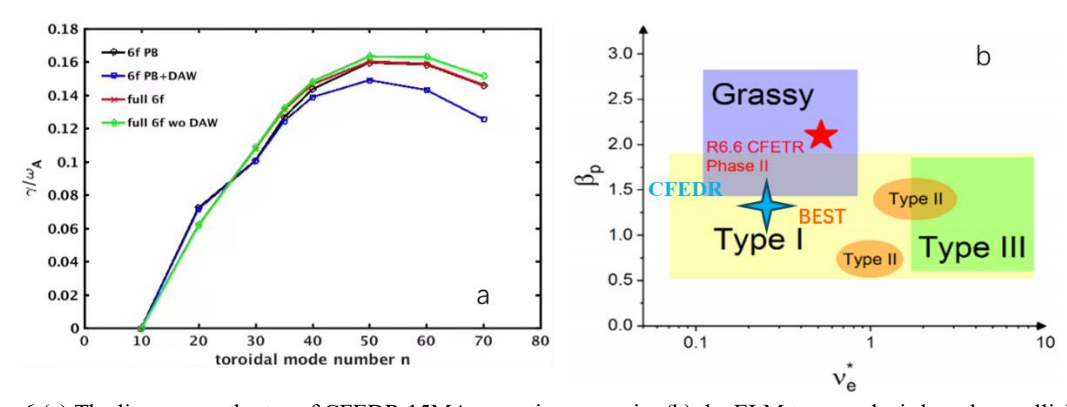


Figure 6 (a) The linear growthrates of CFEDR 15MA operation scenario. (b) the ELM type analysis based on collisionality and  $\beta_p$ .

The linear analysis is shown in Figure 6(a). This equilibrium is highly unstable to ideal PBM, the resistivity and DAW plays little effects on the final linear growthrates. This linear characteristic is similar to the ELM type estimation in Figure 6(b), so it is supposed to be a Type-I ELM.

However, for the nonlinear simulations, similar to the previous conclusion, the ELM size calculated by the full model is only 0.16%, which should be in the grassy/small ELM regime. Different from the previous section, the decrease of ELM size is not from the linear behaviour of compressible terms, but from the nonlinear interactions between PBM and DAW. This interaction has been studied in the studies of grassy ELMs in DIII-D and EAST [26,27]. The mitigation effects by modelled turbulence on ELMs in EAST are also reproduced with elm-6f module in Ref [23]. In this work, if we turn off the DAW driving terms from the model, the simulated ELM size is increased to 0.68%, more than 4 times larger than that of the case with DAW. Although this ELM size is still

in small ELM regime, the interacting between DAW and PBM is still able to decrease the energy loss and transient heat flux dramatically, which is benefit for the plasma facing materials.

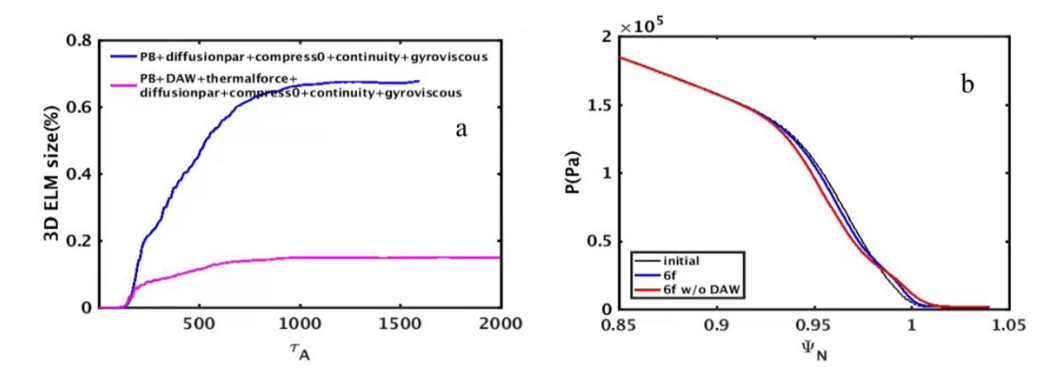


Figure 7 (a) The evolution of ELM size for CFEDR with (magenta) and without (blue) DAW. (b) The pressure profiles at the quasi-steady state in the simulations for with (blue) and without (magenta) DAW.

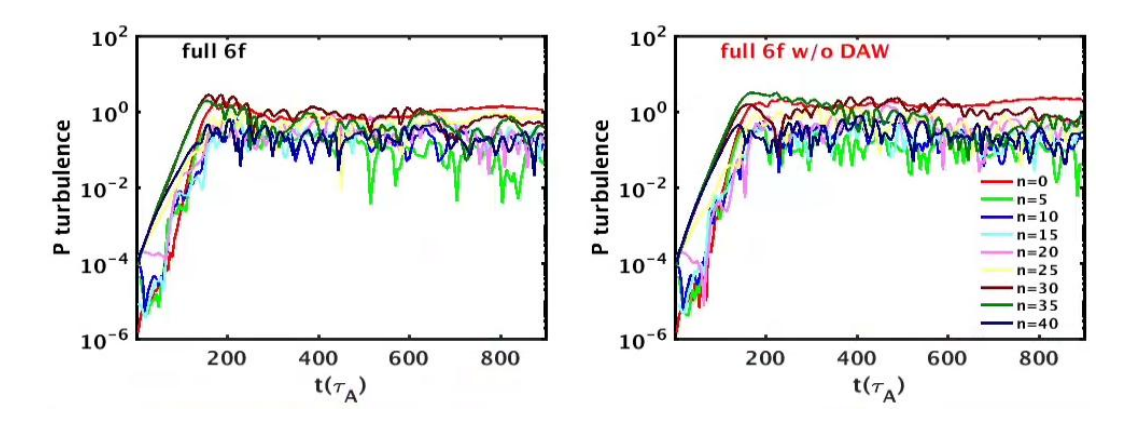


Figure 8 Left: the evolution of pressure fluctuations with different toroidal mode number n with the full 2-fluid model in elm-6f. Right: the evolution of pressure fluctuations with different n just without DAW.

Figure 8 shows the comparisons of the pressure fluctuations of different toroidal mode number between the cases with and without DAW. For both cases, n=35 becomes dominant in the linear and the entrance of the nonlinear phase. The n=30 mode is dominant when the case with DAW is in the early nonlinear phase, then it is still larger than the zonal component until t~650  $\tau$ <sub>A</sub>. For the without DAW case, the n=35 is dominated the system until t~400  $\tau$ <sub>A</sub>. After that the zonal component is the largest mode which is tightly related to ELM size. The detailed analysis will be shown in the presentation of the conference.

# 5. SUMMARY

In this work, we present the ELM simulations of ITER, a JET-size-like tokamak and CFEDR. The linear and nonlinear analysis on PFPO-2 of ITER, 7.5MA high performance scenario of the JET-size-like tokamak and 15MA scenario of CFEDR are exhibited. All the pedestals are linearly unstable to ideal PBM and DAW does not play important roles. For the nonlinear simulations, all the three equilibria obtain the small ELM regime. DAW plays different roles in the nonlinear analysis. In PFPO-2, the absence of DAW leads to no profile crash, while for CFEDR, it leads to larger collapse of pressure. This discrepancy is due to the different nonlinear interaction between DAW and PBM.

#### **ACKNOWLEDGEMENTS**

This work is supported by the National Natural Science Foundation of China (Grant Nos. 12175275), the China Postdoctoral Science Foundation (Grant Nos. 2023M733545, 2023M743541), the Postdoctoral Fellowship Program of CPSF (Grant No. GZC20232714), the CASHIPS Director's Found (Grant Nos. YZJJ2023QN18, YZJJ2024QN26, YZJJ2024QN23), the Anhui Provincial Natural Science Foundation (Grant No. 2408085MA004), and the Science Foundation of ASIPP (Grant No. DSJJ-2023-01). This work is also sponsored in part by the Youth Innovation Promotion Association Chinese Academy of Sciences (Y2021114), Numerical computations were performed on Hefei advanced computing center, the ShenMa High Performance Computing Cluster in Institute of Plasma Physics, Chinese Academy of Sciences.

## REFERENCES

- [1] P.B. Snyder et al, Nucl. Fusion 49 (2009) 085035.
- [2] A.W. Leonard, Phys. Plasmas 21 (2014) 090501.
- [3] T.E. Evans et al. Phys Rev Lett 92 (2004) 235003
- [4] Y.M. Jeon et al. Phys Rev Lett 109 (2012) 035004
- [5] Y.F. Liang et al. Phys Rev Lett 98 (2007) 265004
- [6] Y. Sun et al. Phys Rev Lett 117 (2016) 115001
- [7] G.T.A. Huijsmans et al. Physics of Plasmas 22 (2015) 021805
- [8] R. Maingi et al. Phys Rev Lett 107 (2011) 145004
- [9] J.S. Hu et al. Phys Rev Lett 114 (2015) 055001
- [10] B.N. Wan et al Nucl. Fusion 55 (2015) 104015.
- [11] X.J. Zhang et al Sci. China-Phys. Mech. Astron. March Vol. 65 No. 3 (2022) 235211.
- [12] Li Y.L. et al Nucl. Fusion 62 (2022) 066043.
- [13] X.Q. Xu et al., Phys. Rev. Lett. 105 (2010) 175005.
- [14] P.W. Xi et al., Phys. Rev. Lett. 112 (2014) 085001.
- [15] T.Y. Xia et al., Nucl. Fusion 53 (2013) 073009.
- [16] H.Y. Guo et al., J. Nucl. Mater. 463 (2015) 528-32.
- [17] T.Y. Xia et al., Nucl. Fusion 55 (2015) 113030.
- [18] X.Q. Xu et al., Phys. Plasmas 23 (2016) 055901.
- [19] Z.X. Liu et al., Phys. Plasmas 23 (2016) 120703.
- [20] X.Q. Xu et al., Phys. Plasmas 20 (2013) 056113.
- [21] C.H. Ma et al., Phys. Plasmas 22 (2015) 055903.
- [22] C.H. Ma et al., Phys. Plasmas 22 (2015) 010702.
- [23] Y.L. Li et al., Nucl. Fusion 62 (2022) 066018.
- [24] S.H. Kim et al Nucl. Fusion 56 (2016) 126002, Nucl. Fusion 58 (2018) 056013.
- [25] P.B. Snyder et al., Phys. of Plasmas, 9(5) (2002) 2037.
- [26] N.M. Li et al., J. Plasma Phys. 90 (2024) 5900117, Nucl. Fusion 62 (2022) 096030, Nucl. Fusion 63 (2023) 124005.
- [27] X.X. He et al., submitted to Nucl. Fusion